Publications

Available Online

J. Sci. Res. **15** (2), 361-370 (2023)

JOURNAL OF SCIENTIFIC RESEARCH

www.banglajol.info/index.php/JSR

Magnetocaloric and Magneto-transport Properties in Polycrystalline $Ni_{56}Mn_{20}Ga_{24}$ Heusler Alloy

D. Pal *

Department of Physics, Gokhale Memorial Girls' College, 1/1 Harish Mukherjee Road, Kolkata, West Bengal, India, PIN 700020

Received 4 September 2022, accepted in final revised form 18 January 2023

Abstract

Polycrystalline ingots of Ni-rich $Ni_{56}Mn_{20}Ga_{24}$ alloy were prepared by conventional arc melting procedure. The magnetocaloric and magnetotransport properties of the alloy were investigated within a temperature range from 4.2-300 K and up to a magnetic field of 8 T. A large magnetocaloric effect (ΔS_M ~ 29 J/Kg K) was observed in the alloy in the vicinity of magneto-structural transition temperature at a change of 5 T magnetic field. From magnetic measurements, it was observed that the martensite to austenite transition was accompanied by higher to lower magnetization in higher magnetic fields. The large entropy change was explained by considering the first-order magneto-structural transition in this alloy. A high negative magnetoresistance (~7 %) associated with magnetic field induced first order magneto-structural transition was also observed near room temperature due to a change of 8 T magnetic field for this alloy.

Keywords: Heusler alloy; MCE; Martensitic transition; Magnetic entropy; Magnetoresistance.

doi: http://dx.doi.org/10.3329/jsr.v15i2.61584 J. Sci. Res. **15** (2), 361-370 (2023)

1. Introduction

To hold up climate change and the reduction of natural resources, research in finding environment-friendly and energy-efficient technologies has gained the utmost importance. As the global power demand for cooling is increasing daily, it has become crucial to develop some energy-efficient, less-expensive, and environment-friendly cooling technology. The magnetocaloric effect can provide a promising alternative technology for cooling in those aspects. In simple terms, the magnetocaloric effect (MCE) is a phenomenon of heating or cooling of a magnetic material under the application of a magnetic field. It was first discovered in Iron by Worberg [1]. Debye [2] and Giauque [3] interpreted the thermodynamics of MCE, and both of them independently suggested that using paramagnetic salts at low temperatures can be achieved by adiabatic demagnetization. Utilizing MCE, the magnetic refrigerator was first demonstrated by Giauque and McDougal [4]. Taking 61 g of $Gd_2(SO_4)_3.8H_2O$ as magnetic refrigerant, they

* *Corresponding author*: deba.phy19@gmail.com

reached the lowest temperature of 0.25 K using a magnetic field of 0.8 T. After that, several advancements occurred regarding MCE and magnetic cooling technology.

Magnetic refrigeration (MR) that uses MCE has become a competitive cooling technology because it does not require any gaseous substance (or hazardous substance) as a refrigerant. It is also an energy-efficient technology. The magnetocaloric effect/property of the refrigerant material, which is defined as the isothermal magnetic entropy change (ΔS_M), determines the cooling efficiency of magnetic refrigeration. The adiabatic temperature change of material under the change of a magnetic field is directly related to ΔS_M [5]. In the search for material with large ΔS_M, V. K. Pecharsky and K. A. Gschneidner, Jr. jointly discovered giant MCE in $Gd_5(Si_2Ge_2)$ [6]. Gadolinium (Gd) rare-earth metal and its compound paramagnetic materials with large MCE is considered the most active magnetic refrigerant in room-temperature magnetic refrigerators, but its usage is somehow commercially limited because the cost of Gd is quite expensive. Therefore, it has become necessary to find alternative materials as efficient magnetic refrigerants. Among the recent magnetocaloric materials, Ni-Mn-based Heusler alloys have attracted immense attention to the researcher as the alloys show large MCE associated with the magneto-structural transition [7-10]. These alloys are also important for their shape memory effect, magnetic field-induced strain, magnetoresistance (MR), etc. [11], which makes them smart materials. They undergo a magneto-structural transition from low-temperature martensite phase (tetragonal in structure) to high-temperature austenite phase (cubic $L2_1$ structure) on heating and reverse the process during cooling [12,13]. Most of these alloys' functional properties, like magnetic field-induced strain, magnetocaloric effect, magnetoresistance, etc., are associated with the first-order magneto-structural transition (FOMST) [14]. The alloy shows a high value of $\partial M/\partial T$ at FOMST, which gives rise to a large value of ΔS_M according to Maxwell's thermodynamic equation of entropy [11]. By proper tuning of the composition of the alloys (Ni-Mn-X) or by substituting suitable atoms in place of Ni, Mn, or X atoms, the structural instability associated with the field-induced first-order structural transition can be varied in a wide range which makes them promising magnetocaloric materials in the room temperature refrigeration [15]. This group of alloys (Ni-Mn-X, X=Ga, In, Sn, Sb) also shows exciting magnetotransport properties near their transition temperatures [16]. However, a large number of research works regarding MCE in Ni-Mn-Ga alloys have been reported in the literature [17-20], but the magnetotransport properties have not been studied so extensively for this alloy. A giant reversible inverse magnetocaloric effect in $Ni_{50}Mn_{35}In_{15}$ Heusler alloy has also been reported by Quetz *et al*. [21]. A maximum adiabatic temperature change of -10.4 K was observed near the magnetostructural phase transition in this alloy. Recently, a large magnetic entropy change of -30 J/Kg. K was reported for an annealed ribbon of $Ni_{52}Mn_{26}Ga_{22}$ alloy at its magneto-multi structural transition [18]. Pal *et al.* reported a large magnetoresistance with a large inverse magnetocaloric effect in $Ni_{52}Mn_{34}Sn_{14}$ Heusler alloy at its first-order magnetostructral transition temperature [22].

In our earlier work, a large MCE (ΔS_M = ~96 J kg^{-1} K^{-1}) in $Ni_{54}Mn_{17}Ga_{29}$ alloy was reported near room temperature, where both the structural transition and Ferro-para

magnetic transition coincide with each other [19]. In this work, polycrystalline $Ni_{56}Mn_{20}Ga_{24}$ alloy was prepared to study the effect of substitution of Mn and Ga by Ni atom. Both magnetocaloric and magnetotransport properties of this alloy near magnetostructural phase transition have also been presented in a systematic way in this paper.

2. Experimental Procedure

The polycrystalline ingot of $Ni_{56}Mn_{20}Ga_{24}$ alloy (Nominal composition) was prepared by conventional arc melting. The arc melted ingot was wrapped by Ta foil and taken in a sealed vacuum quartz ampoule. Then it was annealed at 1273 K for 72 h for homogenization. After annealing, the ampoule was quenched in ice water. The final composition of the alloy was determined by energy-dispersive spectroscopy (EDS) and was found to be very slightly different from that of the nominal composition of the alloy. To confirm the phase purities of the alloy x-ray powder diffraction pattern (XRD) was carried out at room temperature using Co-Kα radiation. The structural transition temperatures were determined from differential scanning calorimetry (DSC) measurement. A superconducting quantum interference device (SQUID) was employed to carry out magnetic measurements up to a maximum magnetic field of 5 T. Magneto-transport properties were performed in a physical properties measurement system (PPMS) by standard four-probe techniques up to a magnetic field of 8 T. The MR was determined using the usual expression $\Delta\rho/\rho_0=(\rho_H-\rho_0)/\ \rho_0$.

2.1. *Materials and instruments*

All the chemicals Ni, Mn, and Ga were procured from Sigma-Aldrich and used without further purification. Arc Melt Furnace- Tri-Arc, MRF, Model TA-200 (USA) was used to prepare the ingot of alloy. EDS was performed using a scanning electron microscope (JEOL, Model JSM IT 800). The X-ray diffraction pattern was taken at room temperature by using an X-ray diffractometer - Philips X'Pert (Co Kα radiation). The differential scanning calorimetry measurement was performed with DSC, Perkin Elmer Pyris 1. A SQUID was employed to measure the magnetic properties of the alloy (Quantum Design, MPMS-5S, North America). Quantum Design PPMS Ever Cool-II (North America) was used to measure the magnetoresistance of the sample.

3. Results and Discussion

The X-Ray diffraction pattern of the sample is shown in Fig. 1. As depicted in the figure, the alloy shows cubic $L2_1$ structures (space group $Fm\bar{3}m$) at room temperature with lattice parameter 5.756 Å as well as NM martensite phase, which is in good agreement with earlier reports [23,24]. As the structural transition temperature of the alloy is close to room temperature, the NM martensite phase is also observed in the XRD pattern. DSC measurements during heating and cooling with a heating/cooling rate of 5 K/min have

been plotted in Fig. 2. An endothermic peak during heating and an exothermic peak during cooling are evident in that figure which indicates the martensite to austenite structural transition and the reverse transition respectively.

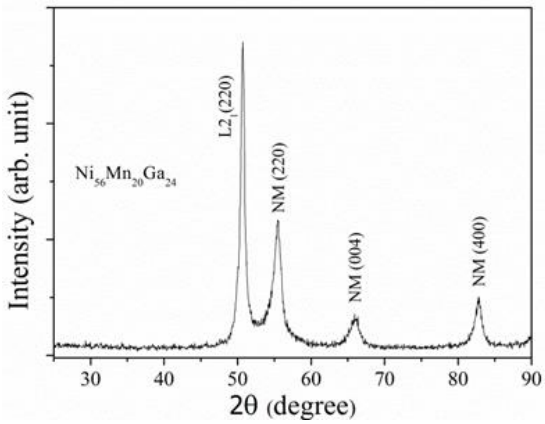

Fig. 1. X-ray powder diffraction pattern of the $Ni_{56}Mn_{20}Ga_{24}$ alloy at room temperature.

The endothermic peak appeared at a lower temperature compared to the exothermic peak. Different transition temperatures, austenite start (A_S), austenite finish (A_F), martensite start (M_S), and martensite finish (M_F) have been marked in Fig. 2. The austenitic transition (transition from the martensite phase to austenite phase) temperature has been calculated by, $T_A = (A_S + A_F)/2$. Similarly, the martensitic transition (transition from the austenite phase to the martensite phase) temperature has been calculated by $T_M = (M_S + M_F)/2$. All the characteristic temperatures obtained from DSC curves have been tabulated in Table 1. Magnetization versus temperature curves of $Ni_{56}Mn_{20}Ga_{24}$ alloy was taken from 4 K to 300 K for both heating and cooling in ZFC condition in the presence of 0.01 T magnetic field and plotted in Fig. 3. During cooling of the sample, a ferromagnetic transition takes place in the Curie temperature T_C=330 K with a sudden large increase in magnetization. A sharp downturn in magnetization was observed at a temperature of 288 K, indicating the start of martensitic transformation from austenite to martensite phase (M_S). On further cooling, an abrupt increase in magnetization is observed around a temperature of 243 K (T_{IM}), revealing another distinct structural transformation called intermartensitic transformation.

The intermartensitic transition is a transformation between two martensite phases with different structures and is usually observed in alloys with T_A or T_C near or higher than room temperature [23-25]. During the same heating, transitions are observed in reverse order. All the transition temperatures obtained from M vs. T curves have been tabulated in Table 1, and comparisons have been made with those obtained from DSC curves. It is found that the austenitic transition temperature (T_A) and martensitic transition temperature (T_M) are almost the same as those obtained from DSE curves and M vs. T curves (Table 1).

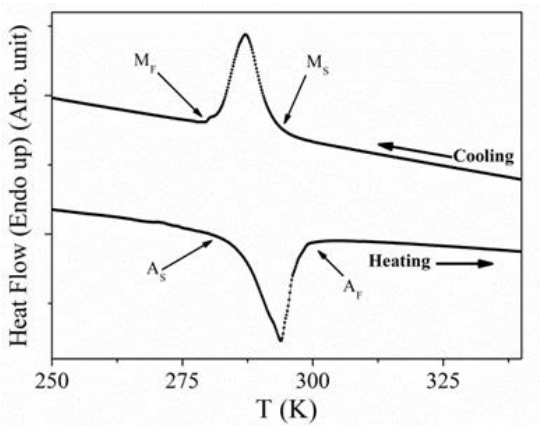

Fig. 2. Differential scanning calorimetry study of the alloy $Ni_{56}Mn_{20}Ga_{24}$ during heating and cooling (rate 5 K/min).

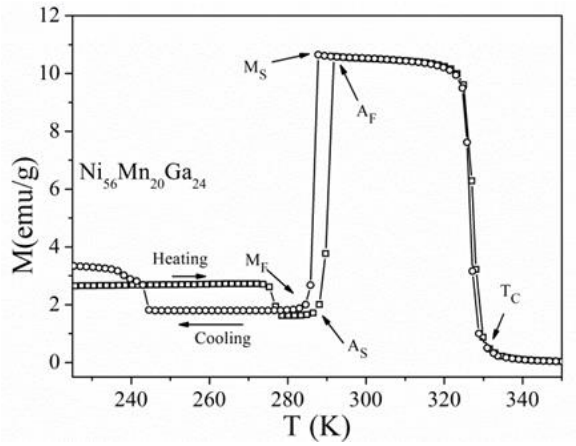

Fig. 3. Thermomagnetic curves of $Ni_{56}Mn_{20}Ga_{24}$ alloy in ZFC condition under 0.01 T magnetic fields during heating and cooling.

Table 1. A_S, A_F, T_A, M_S, M_F, $T_{M,}$ $T_{IM,}$ and T_C of $Ni_{56}Mn_{20}Ga_{24}$ alloy.

	All temperatures are in K								
	A_S	A_F	T_A	M_S	M_F	T_M	T_{IM} (Heating)	T_{IM} (Cooling)	T_C
Obtained from the DSC curve	279	301	290	295	280	288	-	-	-
Obtained from the thermomagnetic curve	284	292	288	288	283	286	273	243	330
Obtained from ρ vs. T curve	289	291	290	291	289	290	270	234	-

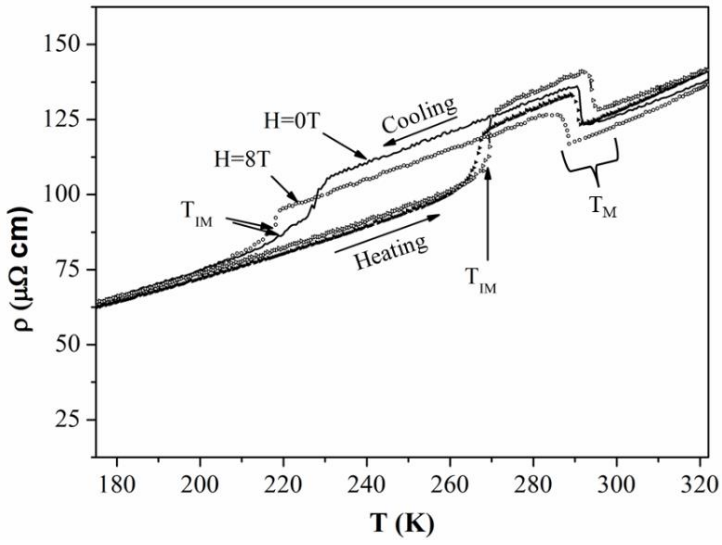

Fig. 4. Resistivity (ρ) vs. temperature (T) data (during heating and cooling) for $Ni_{56}Mn_{20}Ga_{24}$ alloy within a temperature range of 180 – 320 K in the absence and in the presence of an 8 T field.

Fig. 4 shows the resistivity (ρ) vs. temperature (T) data (both heating and cooling) for $Ni_{56}Mn_{20}Ga_{24}$ alloy within a temperature range of 180 – 320 K in the absence and in the presence of an 8 T field. Intermartensitic/martensitic transitions can be identified by discontinuous changes of resistivity in the curves. In the ρ vs. T curve (during cooling; H=0 T), a large increase in resistivity at 291 K corresponds to the austenite-martensite transformation. A downturn in this resistivity curve at 234 K also indicates the intermartensitic transformation, as evident from the M vs. T graph. On subsequent heating, similar transformations are observed, but in reverse order with some hysteresis effect for both the transitions (T_M and T_{IM}). The magnetic field-induced shift in transition temperatures is evident from the curves which correspond to FOMST in this alloy. The transition temperatures shifted towards lower temperatures when the magnetic field of 8T was applied. The shift in transition temperature per magnetic field (dT_M/dH) was found to be -0.5 K/T. The different transition temperatures obtained from these curves are almost identical to those obtained from DSC and M vs. T, as tabulated in Table 1.

The martensitic transition temperature depends on the alloy's valance electron concentration (e/a). The e/a value was calculated from the chemical formula of the compound and found to be 7.72 in this alloy. The martensitic transition temperature for this e/a value of the alloy agrees well with that obtained by other researchers [26]. It has also been established that the hybridization of 3d states of Ni and Mn is also responsible for martensitic transition temperature [27]. The martensite–austenite transition temperature of our sample is much lower than the reported value of $Ni_{55.8}Mn_{18.1}Ga_{26.1}$ alloy because of the addition of extra Ni atoms in the regular Mn sites [28]. This is due to the addition of extra Ni atoms in the regular Mn sites. In the off-stoichiometric Heusler

structure, the Mn atoms in the regular Mn site interact anti-ferromagnetically with the excess Mn atoms in the Ga site. This AFM interaction stabilizes the martensite phase to a higher temperature. It is well established that the substitution of Ni, Co, or Fe in the Mn site enhances the ferromagnetic exchange interaction and diminishes antiferromagnetic coupling between Mn atoms in regular Mn sites and Mn atoms in Ga sites in the martensite phase, which in turn decreases the T_M. This fact explains the lower value of martensite-austenite transition temperature in our sample in comparison to $Ni_{55.8}Mn_{18.1}Ga_{26.1}$ alloy.

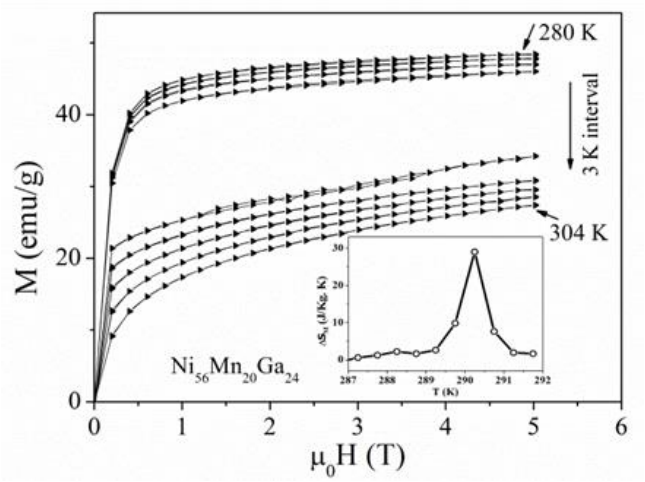

Fig. 5. Magnetic isotherms of $Ni_{56}Mn_{20}Ga_{24}$ alloy from 280 to 304 K at the interval of 3 K.

Magnetic isotherms of the sample around structural transition temperature (290 K) were measured at 3 K temperature intervals and up to a maximum magnetic field of 5 T (Fig. 5). change of magnetic entropy has been calculated from these curves using Maxwell's thermodynamic relations: Eq. (1) [11].

$$\Delta S_M = \int_0^H \left(\frac{\partial M(T,H)}{\partial T}\right)_H dH, \quad (1)$$

Using this equation, calculated ΔS_M values at different temperatures are shown in the inset of Fig. 5. Large Change in magnetic entropy of -29 J/Kg. K obtained at 290.5 K. Difference in saturation magnetizations between martensite and austenite phase ($\Delta M = M_{Martensite} - M_{Austenite}$) causes large entropy change. It is also increased with increasing Ni content [29]. Excess Ni atoms in this alloy increase the Ni-Mn and Mn-Mn ferromagnetic exchange interaction at both austenite and martensite phases [30]. The large difference in saturation magnetization (ΔM) between the two states may be due to ferromagnetic and antiferromagnetic exchange interaction in the Mn-excess and regular-Mn atoms at the austenite state and martensite state, respectively, which causes the large entropy change at the first order magneto-structural transition.

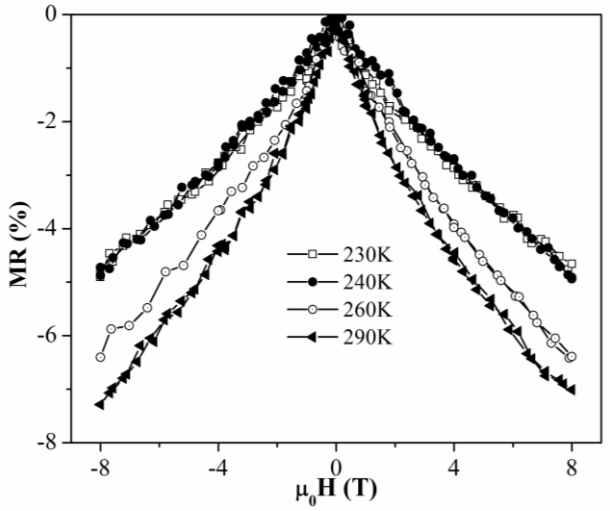

Fig. 6. Isothermal MR curves of $Ni_{56}Mn_{20}Ga_{24}$ alloy at temperatures 230, 240, 260, and 290 K.

From ρ vs. T curves (Fig. 4), it was observed that the resistivity of the alloy decreases under the application of an 8 T magnetic field in a temperature range from 230-300 K during cooling. It is also evident from the curves that in the cooling cycle, the sample goes through martensitic and intermartensitic transitions around 290 K and 230 K, respectively. Therefore, to find a high MR value and to observe the behavior of MR near transition temperatures, data for isothermal MR curves at temperatures 230, 240, 260, and 290 K have been taken during the cooling of the sample and plotted in Fig. 6. A maximum negative MR of ~7% was obtained when the sample is about martensitic transition temperature 290 K. Near the onset of magnetic order, the scattering of charge carriers by magnetic fluctuations can substantially increase electrical resistance, that can be suppressed by a magnetic field, leading to a negative MR [31]. The nonlinear nature of the MR(H) curves is observed when the sample temperature is near the martensitic transition temperature. However, the linearity of the MR(H) curves is observed when the temperatures are far from T_M. At a temperature far below $T_{C,}$ the MR of stable ferromagnets with localized moments and high carrier concentration has been calculated by Kataoka [32] on the basis of scattering between s-conduction electrons and localized d-spins, commonly known as s-d scattering, where a linear variation of MR with filed is shown. Majumdar and Littlewood derived a relation for the MR curves near magnetic transition by scattering rate in the magnetic systems: $\Delta\rho/\rho = C(M/M_S)^2$, which explains the nonlinearity of the curves near martensitic transition [33]. Where M_S is the saturation magnetization, C is given by $(n)^{-2/3,}$ and n is the number of charge carriers per magnetic unit cell. In Ni-Mn-based Heusler alloys where the magnetic field-induced martensitic transition occurred, associated with large resistivity change near transition temperature, showed giant MR [22]. The negative value of dT/dH also manifested the high value of MR near T_M in this alloy, as observed by Khan *et al*. [34]. Furthermore, the spin disorder

scattering is larger in the cubic austenite phase than in the modulated martensitic phase, which also signifies the increasing MR towards the martensitic transition.

4. Conclusion

A large change in magnetic entropy (ΔS_M ~ -29 J/Kg. K) in $Ni_{56}Mn_{20}Ga_{24}$ has been observed near room temperature. The significant change in saturation magnetizations between the martensite and austenite phase ($\Delta M=M_{Martensite}-M_{Austenite}$) at martensitic transition due to the enhancement of ferromagnetic exchange interaction in both phases causes a large entropy change. The shift in martensitic transition temperature observed from ρ vs. T curves due to the application of magnetic field confirmed FOMST. MR of the sample increases with temperature due to the increase of s-d scattering with temperature as a magnetic field suppresses it. A high negative MR of ~7 % was observed for the alloy near the martensitic transition. This large MR in this alloy near T_M is associated with magnetic field-induced FOMST and due to spin disorder scattering.

Acknowledgment

A part of this work was performed at S. N. Bose National Centre for Basic Sciences, Kolkata.

References

1. E. Warburg, Annalen der Physik, **13**, 141(1881). https://doi.org/10.1002/andp.19314030502
2. P. Debye, Ann. Phys. **81**, 1154 (1926). https://doi.org/10.1002/andp.19263862517
3. W. F. Giauque, J. Amer. Chem. Soc. **49,** 1864 (1927). https://doi.org/10.1021/ja01407a003
4. W. F. Giauque and D. P. McDougall, Phys. Rev. **43**, 768 (1933). https://doi.org/10.1103/PhysRev.43.768
5. H. A. Morrish, The Physical Principles of Magnetism (New York: Wiley (1965) pp. 78–83.
6. V. K. Pecharsky and K. A. Gschneidner Jr. Phys. Rev. Lett. **78**, 4494 (1997). https://doi.org/10.1103/PhysRevLett.78.4494
7. V. Basso, C. P. Sasso, K. P. Skokov, O. Gutfleisch, and V. V. Khovaylo, Phys. Rev. B **85**, ID 014430 (2012). https://doi.org/10.1103/PhysRevB.85.014430
8. B. Ingale, R. Gopalan, M. R. Manivel, and V. Chandrasekaran, Appl. Phys. **102**, ID 013906 (2007). https://doi.org/10.1063/1.2751489
9. F. Zhang, I. Batashev, N. V. Dijk and E. Bruck, Phys. Rev. Appl. **17**, ID 054032 (2022). https://doi.org/10.1103/PhysRevApplied.17.054032
10. A. Ahmad, S. Mitra, S. K. Srivastava, and A. K. Das, J. Phys. D: Appl. Phys. **54**, 385001 (2021). https://doi.org/10.1088/1361-6463/ac0aba
11. R. Kainuma, Y. Imano, W. Ito, Y. Sutou, H. Morito, S. Okamoto *et al*. Nature **439**, 957 (2006). https://doi.org/10.1038/nature04493
12. T. Krenke, E. Duman, M. Acet, E. F. Wassermann, X. Moya, L. Manosa, and A. Planes, Nature Mater. **4**, 450 (2005). https://doi.org/10.1038/nmat1395
13. E. T. Dilmieva, Y. S. Koshkid'ko, V. V. Koledov, V. V. Khovaylo, J. Cwik, V. G. Shavrov, and V. Sampath, J. Appl. Phys. **127**, 175103 (2020). https://doi.org/10.1063/5.0003287
14. J. Liu, T. Gottschall, K. P. Skokov, J. D. Moore, and O. Gutfleisch, Nature Mater. **11**, 620 (2012). https://doi.org/10.7312/li--16274-011

15. F. Zhang, I. Batashev, N. Dijk, and E. Bruck, Phys. Rev. Appl. **17**, ID 054032 (2022). https://doi.org/10.1103/PhysRevApplied.17.054032
16. M. Khan, A. K. Pathak, M. R. Paudel, I. Dubenko, S. Stadler, and N. Ali, J. Magn. Magn. Mater. **320**, L21 (2008). https://doi.org/10.1016/j.jmmm.2007.06.016
17. Z. Li, Y. Zhang, C. F. Sanchez-Valdes, J. L. Sanchez Llamazares, C. Esling, X. Zhao, and L. Zuo, Appl. Phys. Lett. **104**, ID 044101 (2014). https://doi.org/10.1063/1.4863273
18. Y. S. Koshkid'koa, E. T. Dilmieva, A. P. Kamantsev, J. Cwik, K. Rogacki et al., J. Alloys Compd. **904**, ID 164051 (2022). https://doi.org/10.1016/j.jallcom.2022.164051
19. D. Pal, J. Sci. Res. **12**, 303 (2020). https://doi.org/10.3329/jsr.v12i3.44357
20. V. V. Khovaylo, K. P. Skokov, S. V. Taskaev, D. Y. Karpenkov, E. T. Dilmieva, V. V. Koledov, Y. S. Koshkid, V. G. Shavrov, V. D. Buchelnikov, V. V. Sokolovskiy, I. Bobrovskij, A. Dyakonov, R. Chatterjee, and A. N. Vasiliev, J. Appl. Phys. **127**, 173903 (2020). https://doi.org/10.1063/5.0003327
21. A. Quetz, Y. S. Koshkid'ko, I. Titov, I. Rodionov, S. Pandey et al., J. Alloys Compd. **638**, 139 (2016). https://doi.org/10.1016/j.jallcom.2016.05.106
22. D. Pal, A. Ghosh, and K. Mandal, J. Magn. Magn. Mater. **360**, 183 (2014). https://doi.org/10.1016/j.jmmm.2014.02.023
23. W. H. Wang, Z. H. Liu, J. Zhang, J. L. Chen *et al*, Phys. Rev. B **66**, ID 052411 (2002). https://doi.org/10.1103/PhysRevB.66.052411
24. I. Babita, M. M. Raja, R. Gopalan, V. Chandrasekaran, and S. Ram, J. Alloys Compd. **432**, 23 (2007). https://doi.org/10.1016/j.jallcom.2006.06.003
25. R. F. Hamilton, H. Sehitoglu, C. Efstathiou, and H. J. Maier, Acta Mater. **55**, 4867 (2007). https://doi.org/10.1016/j.actamat.2007.05.003
26. J. Marcos, L. Mañosa, A. Planes, F. Casanova, X. Batlle, and A. Labarta, Phys. Rev. B **68**, ID 094401 (2003). https://doi.org/10.1103/PhysRevB.68.094401
27. M. Ye, A. Kimura, Y. Miura, M. Shirai, Y.T. Cui, K. Shimada, H. Namatame, M. Taniguchi, S. Ueda, K. Kobayashi, R. Kainuma, T. Shishido, K. Fukushima, and T. Kanomata, Phys. Rev. Lett. **104**, 176401 (2010). https://doi.org/10.1103/PhysRevLett.104.176401
28. Z. Li, K. Xu, Y. Zhang, C. Tao, D. Zheng, and C. Jing, Sci. Rep. **5**, ID 15143 (2015). https://doi.org/10.1038/srep15143
29. S. Aksoy, M. Acet, P. P. Deen, L. Manosa, and A. Planes, Phys. Rev. B **79**, ID 212401 (2009). https://doi.org/10.1103/PhysRevB.79.212401
30. A. Ghosh and K. Mandal, J. Phys. D: Appl. Phys. **46**, ID 435001 (2013). https://doi.org/10.1088/0022-3727/46/43/435001
31. M. E. Fisher and J. S. Langer, Phys. Rev. Lett. **20**, 665 (1968). https://doi.org/10.1103/PhysRevLett.20.665
32. M. Kataoka, Phys. Rev. B 63, 134435 (2001). https://doi.org/10.1103/PhysRevB.63.134435
33. P. Majumdar and P. Littlewood, Nature **395**, 479 (1998). https://doi.org/10.1038/26703
34. M. Khan, I. Dubenko, S. Stadler, and N. Ali, J. Phys.: Condens. Matter **20**, ID 235204 (2008). https://doi.org/10.1088/0953-8984/20/23/235204